81-GT-77

AN ASME PUBLICATION
$4.00 per copy $2.00. So AWE Members

THE AMERICAN SOCIETY OF MECHANICAL ENGINEERS
345 E 47 St., New York, N.Y. 10017

Streamwise Flow and Heat Transfer Distributions for Jet Array Impingement with Crossflow

L. W. Florschuetz
Professor
Mem. ASME

C. R. Truman
Graduate Student
Student Mem. ASME

D. E. Metzger
Professor
Mem. ASME

Department of Mechanical Engineering,
Arizona State University,
Tempe, Ariz.

Two-dimensional arrays of circular jets of air impinging on a heat transfer surface parallel to the jet orifice plate are considered. The air, after inpingement, is constrained to exit in a single direction along the channel formed by the surface and the jet plate. The downstream jets are subjected to a crossflow originating from the upstream jets. Experimental and theoretical results obtained for streamwise distributions of jet and crossflow velocities are presented and compared. Measured Nusselt numbers resolved to one streamwise hole spacing are correlated with individual spanwise row jet Reynolds numbers and crossflow-to-jet velocity ratios. Correlations are presented for both inline and staggered hole patterns including effects of geometric parameters: streamwise hole spacing, spanwise hole spacing, and channel height, normalized by hole diameter. The physical mechanisms influencing heat transfer coefficients as a function of flow distribution and geometric parameters are also discussed.

NOMENCLATURE

A — coefficient of Reynolds number in power function fit or correlation equations

A: = ratio of jet hole area to opposing heat transfer surface area (open area ratio)

b = thickness of jet plate

B = coefficient in crossflow function of correlation equation

0 = flow distribution parameter introduced following Eq. (7), CD 112 (n/4)/[y_n/d)/(z/d)]

C = constant appearing in correlation equation

CD — jet plate discharge coefficient

d — jet hole diameter

G_c — channel crossflow mass velocity based on channel cross—sectional area

Gj = jet mass velocity based on jet hole area

= superficial jet mass velocity based on jet plate or equivalent opposing heat transfer surface area

h = convective heat transfer coefficient resolved in streamwise direction, averaged across span

= spanwise hole row number

k = thermal conductivity of fluid

L = streamwise length of heat transfer surface

m = Reynolds number exponent in power function fit or correlation equation

M = flow distribution parameter introduced at Eq. (4), a A:CD/z

[= dynamic viscosity

n = exponent in crossflow function of correlation equation

n_x, n_y, n_z = constants appearing in correlation equation

Nu = Nusselt number resolved in streamwise direction, averaged across span, hd/k

Nu, = value of Nu at first upstream spanwise row of holes where G_c/Gj = 0

N_c number of spanwise rows in streamwise direction

N_s number of jet holes across span of heat transfer surface

N; = number of jet holes across span of channel

P = channel pressure

Po = plenum pressure

Pr = Prandtl number

Rej — jet Reynolds number, Gjd/p

p — fluid density

x — streamwise location along heat transfer surface measured from upstream end of channel

x_n — streamwise jet hole spacing

Yn = spanwise jet hole spacing

z = channel height (jet plate—to—impingement surface spacing)

Superscripts

= overbar refers to mean value

Contributed by the Gas Turbine Division of THE AMERICAN SOCIETY OF MECHANICAL ENGINEERS for presentation at the Gas Turbine Conference & Products Show, March 9-12, 1981, Houston, Texas. Manuscript received at ASME Headquarters December 11, 1980.

Copies will be available until December 1, 1981.

INTRODUCTION

Impingement with high velocity gas jets has become an established method of convectively cooling or heating surfaces in a wide variety of process and thermal control applications. Examples include cooling of gas turbine airfoils and electronic equipment, drying of paper and textiles or other thin layers or films, annealing of metals, and glass tempering operations.

For gas turbine airfoils a significant application utilizing a two—dimensional array of jets is the cooling of the midchord region with a trailing edge discharge. The jet air, after impingement, is constrained to flow toward the rear of the airfoil along the channel formed between the jet orifice plate and the inner surface of the airfoil envelope. Thus, in this configuration, exhaust from the upstream jets imposes a confined crossflow on the downstream jets.

An investigation, supported by the National Aeronautics and Space Administration, was initiated with the primary objective of determining heat transfer behavior for a variety of uniformly spaced impingement array configurations which model those of interest in current and contemplated gas turbine airfoil cooling applications. Earlier publications based on this project presented results for both array mean Nusselt numbers and spanwise averaged, streamwise resolved Nusselt number profiles for arrays having 10 spanwise rows of holes [1,2,3]. These results were for streamwise resolutions from one—third to twice the streamwise hole spacing, and were presented in terms of array mean jet Reynolds numbers and geometric parameters. Results for arrays with both inline and staggered hole patterns were included.

Subsequently, the use of a simple one—dimensional momentum flux model was found to quite accurately predict the row—by—row streamwise flow distributions. In this paper both development of the model and experimental determination of the flow distributions are presented and the results compared. These flow distributions then provide the means by which the spanwise averaged, streamwise resolved Nusselt numbers are examined as a function of the individually associated spanwise row jet Reynolds numbers and crossflow—to—jet velocity ratios. Correlations are presented for both inline and staggered hole patterns for Nusselt numbers resolved to one streamwise hole spacing. Specifically, these Nusselt numbers are correlated in terms of the individual spanwise row jet Reynolds number (Red) and crossflow—to—jet velocity ratio ($G_c/G3$); and in terms of three geometric parameters: the streamwise hole spacing, the spanwise hole spacing, and the channel height each normalized by hole diameter (x_n/d, y_n/d, and z/d). The overall ranges of these variables are Red, 2.5x10^3 to 7x10^4; G_c/Gj, zero to 0.8; x_n/d, 5 to 15 for inline hole patterns and 5 to 10 for staggered patterns; y_n/d, 4 to 8; and z/d, 1 to 3. The aspect ratios, x_n/y_n, for the jet plates ranged from 0.625 to 3.75.

EXPERIMENTAL FACILITY

Only a brief description of the test facility is given here, though a complete summary of the significant characteristics of the jet array geometries tested is included. Additional details may be found in [1] and [2], with complete details available in [3].

The test facility consists overall of a compressed air supply, an air flow metering section, and interchangeable plenum/jet plate assemblies which produce arrays of jets impinging on an instrumented heat transfer test surface. Chordwise (i.e., streamwise) and spanwise cross—sectional views of the assembly of the major components are shown in Fig. 1 for one plenum size. A single test plate unit consisting of a segmented copper test plate with individual segment heaters, the necessary thermal insulation, and the test plate support structure, is utilized for all tests. The segmented design provides for control of the streamwise thermal boundary condition at the heat transfer test surface, as well as for determination of spatially resolved heat transfer coefficients in the streamwise direction. The jet plate under test, positioned by the jet plate holder, is bolted to the lower flange of the plenum, which in turn, is bolted to the test plate unit. The jet plate lower surface is positioned relative to the heat transfer surface via interchangeable spacers to permit covering the desired range of z/d.

Laboratory compressed air is piped to the plenum and passed through the plenum packing to provide a uniform flow upstream of the jet plate. After passing through the jet plate the air exhausts to atmospheric pressure by flowing along the channel formed by the jet plate, the test surface, and the spacer.

There are four interchangeable plenums, each of a different streamwise length. Thus, the channel length varies depending on the size of the particular plenum/jet plate assembly being utilized. The thermally active length of the test plate consists, for a given test, of those test plate segments which are immediately opposite the jet plate. The maximum active chordwise length is 38.1 cm (15 in.) (30 segments by 1.27 cm (0.5 in.) per segment), with an additional segment at the downstream end to serve as a guard element. For tests in which only a fraction of the test plate was thermally active the segment immediately downstream of the active portion served as a guard element.

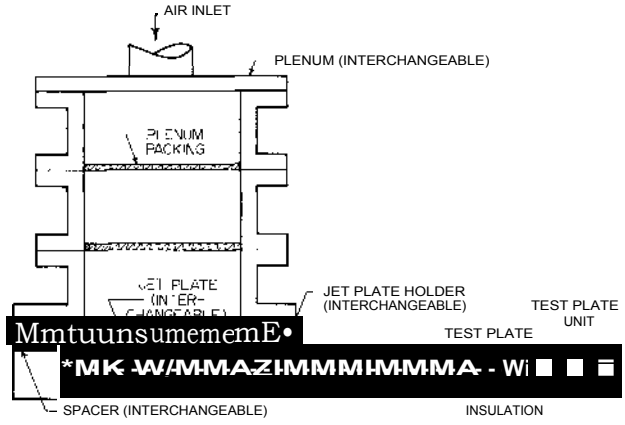

CHORDWISE VIEW

SPANWISE VIEW

Fig.1 Test unit assembly

The jet plate thickness, b, at each hole location is equal to the jet hole diameter. This was achieved by appropriately counterboring plates of larger overall thickness (Fig. 1). This design feature was dictated primarily by the need to insure accurate channel heights during test runs, a particularly critical requirement for the narrowest channel height (.0635 cm). The counterbore was three jet hole diameters, except for the narrowest hole spacing where two jet hole diameters was used. In one test with z/d = 1, a 2d counterbore plate was used with the counterbored holes subsequently bored out to 3d, and the test repeated. The results were identical to within experimental uncertainty.

The significant dimensions and geometric characteristics unique to the interchangeable plenums and matching jet plates for which data was obtained are summarized in Table 1. The smallest jet hole diameter is near prototype size for the gas turbine application, while the larger sizes provided for improved streamwise resolution of heat transfer coefficients. Emphasis in this paper is placed on results from the B, C, and D sizes since, for these, heat transfer coefficients can be resolved to at least one streamwise hole spacing. Note that the number of spanwise rows of holes was fixed at 10 for all jet plates. The first row (counting from upstream) was always displaced $x_n/2$ from the upstream end of the channel. Each jet plate with a staggered hole pattern was identical to its inline counterpart, except that alternating spanwise rows were offset by one-half the spanwise hole spacing. Each individual configuration tested can be uniquely identified by specifying a size designation (A, B, C, or D), a set of geometric parameters ($x_n/Cy_n/d$,z/d), and a hole pattern (I or S). For brevity, specific configurations will be referred to by designations such as B(5,8,2)I; or when it is unnecessary to indicate in this way a specific size, hole pattern, and/or geometric paramter value, obvious notations such as B(5,8)I, B(5,8), or simply (5,8) will be used.

Attention is called to the fact that a number of the configurations of different sizes listed in Table 1 are geometrically similar. Considering sizes B, C, and D the maximum length scale factor is 3; including A-size, the maximum factor is 6.

The discharge coefficients summarized in Table 1 were employed in determination of the row-by-row streamwise flow distributions, as discussed in the next section.

FLOW DISTRIBUTION

The determination of the distribution of the jet flow among the individual spanwise rows was an essential step prior to attempting correlation of the streamwise resolved heat transfer coefficients with the individual row jet and crossflow rates. The flow distributions were determined from measured streamwise channel pressure profiles and jet plate discharge coefficients. A one-dimensional incompressible momentum flux model was also developed which predicted the experimentally determined flow distributions quite satisfactorily.

Experimental

Streamwise channel pressure traverses were accomplished with static pressure probes inserted from the downstream end of the channel. The probes were stainless steel tubes of 0.0635 to 0.124 cm (0.025 to 0.049 in.) outside diameter closed at the upstream end, with a single orifice of 0.0254 cm (0.010 in.) diameter located 0.318 cm (1/8 in.) from the end. For a given run the tube was positioned along one lower corner of the channel and pressed against the channel side wall and bottom by slightly bowing the tube.

Table 1. Geometric characteristics of configurations tested

Plenum Size	L cm (inches)	d & b cm (inches)	xn/d	y_n/d	z/d	Hole Patterns	CD Ns	Ns	C_D I	C_D S	4 of Active Segments	Maximum Chordwise Resolution	Channel Length cm (inches)
A	6.35(2.5)	0.0635(0.025)	10	6	1, 2, 3,6	I,S	32	48		0.80	5	2x,	10.8(4.25)
				8	1,2,3	I	24	36	0.83	--			
B	12.7(5.0)	0.254(0.100)	5	4	1,2,3	I,S	12	18	0.85	0.85	10	xn	17.1(6.75)
				8	1,2,3,6	I,S	6	9	0.80	0.79			
		0.127(0.050)	10	4	1,2,3	I,S	24	36	0.76	0.73			
				8	1,2,3	I,S	12	18	0.76	0.74			
C	25.4(10.0)	0.508(0.200)	5	4	1,2,3	I	6	9	0.81	--	20	$\frac{1}{11}x_n$	29.8(11.75)
				6	1,2,3	I	4	6	0.77	--			
				8	1,2,3	I,S	3	4	0.78	0.78			
		0.254(0.100)	10	4	1,2,3	1,5	12	18	0.82	0.83			
				6	1,2,3	I	8	12	0.79	--			
				8	1,2,3	I,S	6	9	0.79	0.80			
D	38.1(15.0)	0.762(0.300)	5	4	1,2,3	I	4	6	0.81	0.79	30	$\frac{1}{3}x_n$	41.3(16.25)
					1, 3	S							
		0.381(0.150)	10	4	1,2,3	I	8	12	0.80	--			
				8	1,2,3	I	4	6	0.78	--			
		0.254(0.100)	15	4	1,2,3	I	12	18	0.83	--			
				6	1,2,3	I	8	12	0.80				
					1,2,3	I	6	9	0.79				

Notes: I denotes inline hole pattern, S denotes staggered.
The number of holes across the test plate span, N,, varies depending on hole spacing; the number along the chord, $N_c = L/x_n$, was fixed at 10 for all tests reported herein.

This positioning provided support of the tube, thus preventing vibration and possible whipping in the presence of a strong channel flow. The larger diameter tubes were used with larger channel heights which were also associated with longer channel lengths, thus requiring a stiffer probe.

For a given traverse the orifice was positioned either facing upward toward the jet plate, downward toward the channel lower surface, or toward the channel sidewall. For each jet plate configuration, three traverses were usually made, each utilizing a different one of these orifice positions. Manometer readings of the channel pressure were made at each spanwise jet row location, midway between jet rows, and at the farthest possible upstream position, x = 0.318 cm (1/8 in.). Comparison of results for the three orifice positions as well as the smoothness of the points in traversing from locations immediately opposite jet rows to midway between rows indicated that dynamic pressure effects were not significant.

A discharge coefficient for each jet plate was determined from a separate test conducted with the plenum/jet plate assembly removed from the test plate unit and discharging directly to the laboratory environment at atmospheric pressure. Plenum pressure and temperature were measured to calculate the ideal flow rate, assuming one—dimensional isentropic compressible flow, while the actual flow rate was determined via the standard orifice in the flow metering section upstream of the plenum. Discharge coefficients were measured over a range of Rej spanning that for which data was obtained in the heat transfer tests. In most cases at least 16 points were taken spread over the necessary range. The results for jet plate B(5,8)I for which the largest number of points was taken are shown in Fig. 2. These CD values are essentially independent of Rej over the range 2.5×10^3 to 5×10^5. The mean value of CD for each jet plate is listed in Table 1. These values were used in determining the flow distributions. While discharge coefficients for individual holes were not determined, each jet plate was checked for flow uniformity with very satisfactory results as detailed in [3].

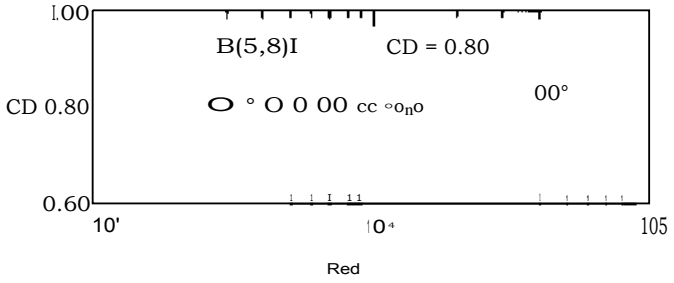

Fig.2 Jet plate discharge coefficients

Results

The distribution of the jet flow as calculated from the pressure traverse and discharge coefficient results is illustrated by the data points in Fig. 3. These points were drawn from the results for the B and C—size configurations, and represent the jet mass velocity for the individual spanwise rows normalized by the mean of the individual values over all ten rows. The sum of the flow rates over all rows closed to within 3% or better of the total flow rate measured upstream of the plenum for all these cases, except one which closed to within 6%. The vertical arrows along the abscissa indicate the row locations. The corresponding points for the crossflow parameter, G_n/Gj, are shown in Fig. 4 [excepting the C(5,6,1)I case, omitted for clarity].

The curves in both Figures are based on the one—dimensional model outlined below. The agreement is quite satisfactory. The model leads to the result that the flow distribution is independent of the streamwise hole spacing, depending, for a given discharge coefficient and number of rows, only on the geometric parameter $(y_n/d)(z/d)$. Data for $x_n/d = 10$ and 15 (not shown in Figs. 3 and 4) verifies this result. The range of this parameter covered in Figs. 3 and 4 matches that for the heat transfer tests. For the largest value, 24, the distribution is essentially uniform with a corresponding linear increase in the crossflow parameter, G_c/Gj. For the smallest value, 4, the distribution is highly nonuniform with the jet velocity as small as one—half the mean at the first row, and as large as twice the mean at the tenth row; G_n/Gi increases linearly upstream but levels off quickly downstream to a maximum value of about 0.75.

Model

The discrete hole array is imagined to be replaced by a surface over which the, injection is continuously distributed (Fig. 5). The jet velocity

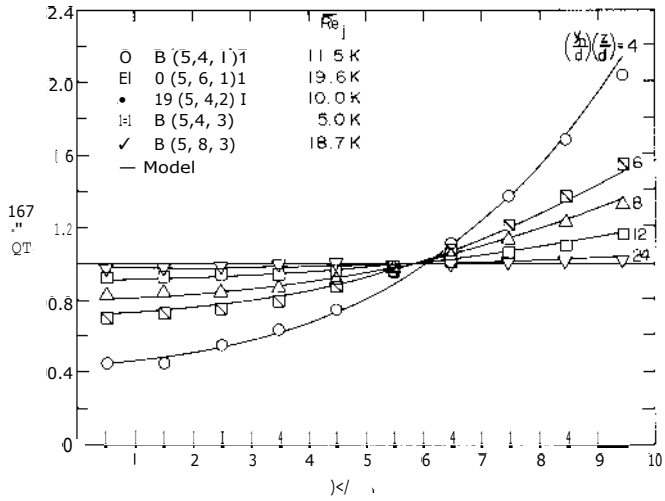

Fig.3 Streamwise distribution of jet velocities--comparison between measured values and model, Eq. (7)

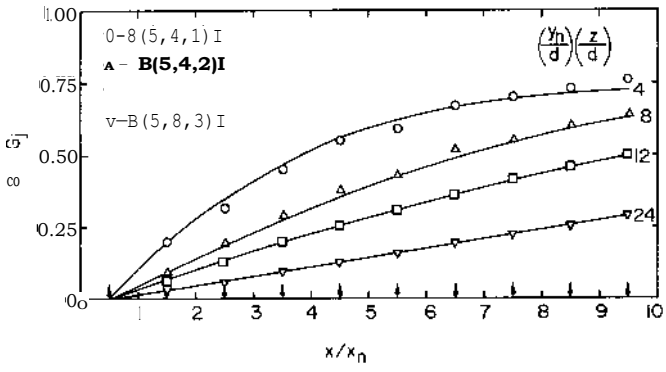

Fig.4 Streamwise distribution of crossflow—to—jet velocity ratio--comparison between measured values and model, Eq. (8)

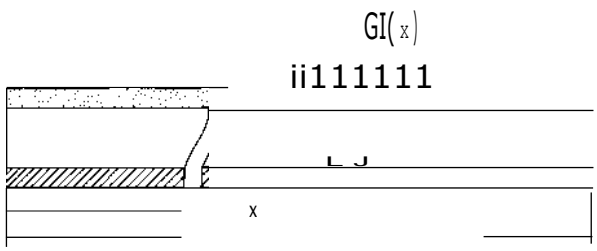

Fig.5a Continuous injection model

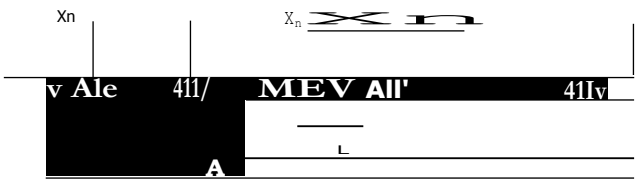

Fig.5b Discrete hole injection model

G_j is related to the continuously distributed injection velocity G: through the open area ratio, e_j = Gi4. Thus, assuming incompressible flow, the distributed injection velocity may be written in terms of the discrete hole discharge coefficient as

$$G: = Ao\ CD\ [2p(P_o-P)1^{1/2}$$

The streamwise pressure gradient in the channel is assumed to be primarily due to the acceleration of the flow caused by the injected fluid, with negligible influence of the wall shear. Accordingly, a force-momentum balance on the control volume indicated in Fig. 5a results in

$$dP = \frac{2GodGo}{p} \qquad (2)$$

A mass balance leads to

$$= z\ \frac{dG}{dx} \qquad (3)$$

For constant CD and P_o, the elimination of GI and P from (1), (2), and (3) in favor of G_o yields

$$\frac{d^2G_o}{dx^2} \quad m2oc = 0 \qquad (4)$$

where $M = V\hat{2}$- Ao CD/z. The upstream boundary condition is G_o = 0 at x = O. A second boundary conditon results from an overall mass balance for a channel length L written in terms of the overall mean injection velocity; i.e., Go = U:Liz at x=1,. Integration of (4) then gives

$$G_o = \frac{L \sinh Mx}{e \quad z \sinh ML} \qquad (5)$$

for the crossflow distribution. The corresponding injected flow distribution obtained from (3) with the aid of (5) is given by

$$\bullet \quad \frac{ML \cosh Mx}{\bullet \quad \sinh ML} \qquad (6)$$

The discrete hole array jet velocity distibution is determined from (6) by assuming that the value of G_j for a given spanwise row of holes is that corresponding to G:(x) with x evaluated at the centerline of the row. For the uniform rectangular arrays of interest here Ao = (n/4)/[(x_n/d)(y_n/d)], L = $x_n N_c$, and the first row is at x = x_n/2. Noting also that $e_j = U_j - A_o$, the jet velocity distribution based on (6), may be written as

$$\frac{G_j \quad 0No \cosh 0(x/x_n)}{U- \quad \sinh 0\ N_o} \qquad (7)$$

where

$$0 = CD\ V2(7/4)/[(y_n/d)(z/d)]$$

and

$$x = x_n(i-1/2) \quad i = 1,2,3 \ldots N_o$$

Besides the jet array velocity distribution given by (7), an additional flow parameter relevant to the correlation of the streamwise resolved heat transfer coefficients is the ratio of the crossflow velocity immediately upstream of a given spanwise row to the jet velocity of that row. This may be satisfactorily approximated utilizing G_o from (5) evaluated one-half a hole spacing upstream of the given row (Fig. 5b), divided by Gj from (7). This results in

$$\frac{G_o = \quad 1 \quad \sinh 0(x/x_n - 1/2)}{Gj \quad V2\ CD \quad \cosh 0(x/x_n)} \qquad (8)$$

where the spanwise hole row locations are the same as previously indicated following (7). The curves shown in Figs. 3 and 4, previously discussed, are based on (7) and (8), respectively.

The one-dimensional model developed above is similar to that presented by Martin [4] for an array of slot nozzles in which the outlet flow is constrained to exit in a single direction parallel to the slots, resulting in continuous injection in the flow direction. The present results indicate the applicability of a one-dimensional model for discrete hole arrays as well.

HEAT TRANSFER COEFFICIENTS

Both mean and streamwise resolved heat transfer coefficients for jet plate configurations summarized in Table 1 were previously presented and discussed as a function of mean jet Reynolds number and geometric parameters [1,2,3]. Heat transfer coefficients resolved to one or two streamwise hole spacings [1,3] and to one-third the hole spacing [2,3] were considered. The experimental procedures and data reduction techniques were outlined in [1] and are further detailed in [3], which includes a complete tabulation of mean and resolved Nusselt numbers. It is noted here that the heat transfer coefficients were determined for an isothermal test surface.

The present objectives are to examine the heat transfer coefficients resolved to one streamwise hole spacing as a function of the associated spanwise row jet velocity, crossflow velocity, and geometric parameters; and to achieve a correlation in terms of these quantities. Thus, we consider

$$h = f(Gj, G_o, x_n, y_n, z, d)$$

or in dimensionless form, taking account also of relevant fluid properties,

$$Nu = f(Rej,\ G_o/Gj,\ Pr,\ x_n/d,\ y_n/d,\ z/d) \qquad (9)$$

Since the flow distribution model presented in the previous section was well supported by the flow

distribution data, this model was used for determination of Re_j and GdGj. It should be emphasized, however, that only the distribution of Rej relative to the mean, i.e., Rej/rij = Gj/Uj was determined from (7). The mean values were taken from the square—edged orifice total flow rate measurements upstream of the plenum since they are more accurate than the sum of the individual row flow rate measurements.

The maximum nominal range of RTj for which heat transfer data was obtained was 5x10³ to 5x10⁴, though the full range was not covered for every individual geometry. Considering the geometries with the most highly nonuniform flow distribution, (y,/d)(z/d) = 4, the maximum nominal range of Rej was 2.5x10³ to 1.75x10⁴ for Row 1 (G_c/Gj = 0) and 10⁴ to 7x10⁴ for Row 10 (G_c/Gj 0.75). For the most nearly uniform flow conditions, (y,/d)(z/d) = 24, the Rej range for all rows (0 G_c/G• 0.28) was essentially the same as the range for **Rej.**

Normally, for a given configuration, heat transfer coefficients were obtained for three values of Ri_j over the range. However, in some cases data were obtained at four or five values while for a few of the C—size geometries data were taken at just two values. Least squares power function fits of the form Nu = A Rem were applied separately to individual data sets, with A and m permitted to be adjustable constants for each set. A data set for this purpose consists of measured Nu values at each Reynolds number for a given geometric size, (x,/d,V_n/d,z/d), hole pattern, and spanwise row. Ninety—five percent of the data points deviated from these fit lines by less than 3%, 99% by less than **4%,** and 100% by less than 9%, which compares quite favorably with the estimated uncertainty for the Nu data which was ±5% for 95% confidence [3]. Thus, the confidence which may be placed in interpolated data points based on these individual fits may be considered as good as that for the original data points. Results based on these fits were used in examining the effects of geometric parameters and crossflow at fixed values of Rej as discussed in the paragraphs below.

Examination of Fig. 6[1] indicates that Nu,, for which G_c/Gj = 0, decreases significantly with both x_n/d and ydd for fixed Rej. The points shown are for Rej = 10⁴; however, the trend with geometric parameters is similar over the Rej range of the tests. The sensitivity to z/d is quite small except for the highest hole density configuration, (xn/d,Ynid) = (5,4), where Nu, for z/d = 1 is significantly larger than the values for z/d = 2 and 3. This is not a spurious data point because the data for the corresponding geometrically similar sizes corroborate this behavior. The trend of Nu, with z/d is decreasing for small values of add and y,/d, but increasing for large values. This type of behavior tends to work against development of a tight correlation of simple form.

Effect of Crossflow

The matrix of plots in Fig. 7 shows the effect of the crossflow parameter, G_c/Gj, on Nu where Nu is normalized by Nu,. Each plot presents results for z/d = 1,2, and 3 for a single hole spacing combination (x,/d, y_n/d). The data shown are for the smallest geometric size tested for that combination (excluding A—size for which Nu could not be resolved to one

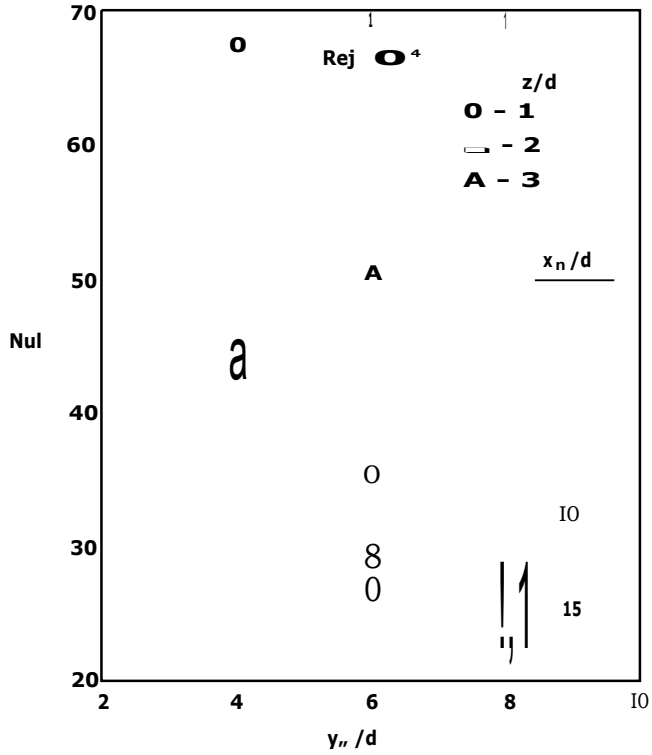

Fig.6 Effect of geometric parameters on Nusselt number for initial upstream row of array. Inline hole pattern.

stremmvisespacing Likupoints, re for Re_j =10⁴ but in this normalized form are representative of the general trends over the full Rej range.

The trend of Nu/Nu, with GdGj shifts from a monotonic decreasing function to a form which exhibits a broad minimum as x_n/d and ydd increase, and as z/d decreases. Thus, for x_{ii}/d 2 10, y,/d 2 6, z/d = 1, and G_e/Gj 2 0.4, Nu/Nu, increases slowly. A plausible explanation for this behavior, consistent with the fact that it occurs for large hole spacings and small channel heights, is that the crossflow provides an increasingly significant direct contribution to the heat transfer rate but does not cause a large degradation in the direct contribution from jet impingement. It may be remarked that results for heat transfer coefficients resolved to better than one streamwise hole spacing indicate that for these geometries the jets at the final downstream row still impinge on the surface; and, indeed, the impingement point is deflected downstream only a small fraction of the hole spacing [2,31. This inference is further corroborated by observations of discoloration patterns on the copper heat transfer surface subsequent to these test runs, which clearly indicate impingement of all jets with only slight deflection even at the final downstream row. In contrast, for smaller hole spacings and/or larger channel heights the jets are deflected and diffused more by the crossflow, and though they still impinge on the heat transfer surface, their cooling effectiveness is more significantly reduced. At the same time there is less surface area available for direct cooling by the cross flow.

The effect of increasing z/d, where significant, is to decrease Nu/Nu, at fixed GdGj. This latter trend is consistent with the results of Metzger and Korstad [5] for a single row of jets tranverse to a crossflow. The sensitivity of Nu/Nu, vs G_c/Gj to z/d

[1] The points for each specific hole spacing combination (add, y,/d) are drawn from the same geometric sizes (B, C, or D) identified in Fig. 7.

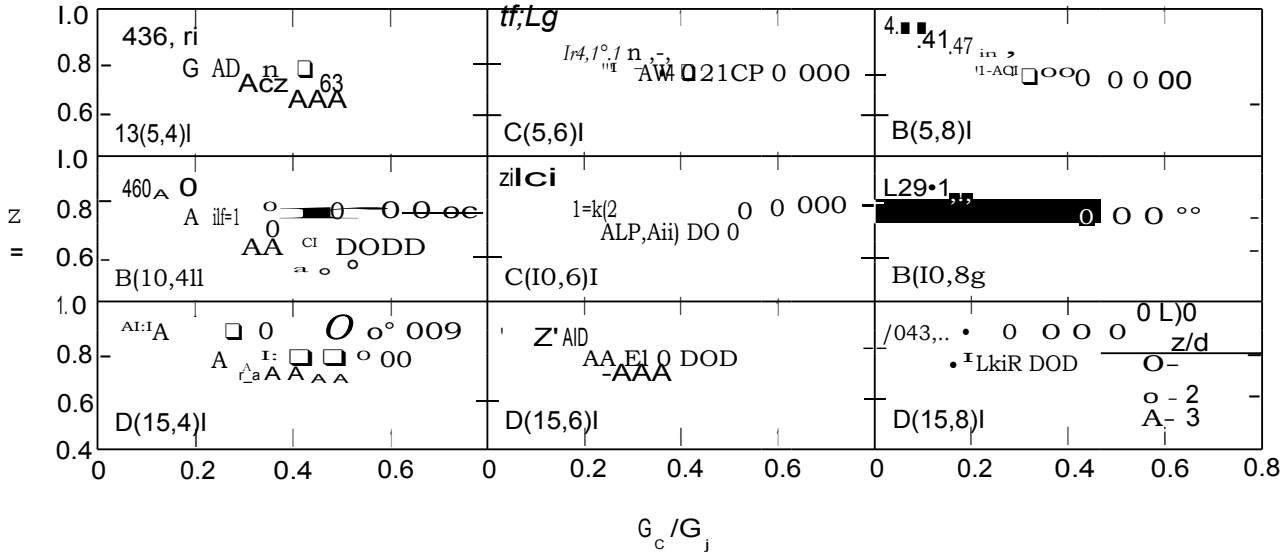

Fig.7 Effect of crossflow and geometric parameters on streamwise resolved Nusselt numbers. Inline hole pattern.

increases with x_n/d but decreases with y_n/d. Thus, the effect of z/d is significant for (x_n/d, y_n/d) = (15,4), the lower left plot, but essentially disappears for (5,8), the upper right plot. Or, stated another way the sensitivity of the crossflow effect to z/d appears to increase as the aspect ratio x_n/y_n increases. The complexity of the interacting jet/crossflow phenomena in the two-dimensional array precludes arriving with high confidence at a particular explanation, at least on the basis of currently available information. However, it may be appropriate to note several factors which contribute to the complexity, and may be involved in potential explanations.

First, the crossflow velocity appearing in the crossflow parameter G_c/Gj as used in characterizing the present results is a mean value over the channel cross-section. Consider the distribution across the channel span of the crossflow velocity averaged over the channel height. There is some evidence, e.g., flow visualization, indicating that for the inline arrays the crossflow tends to become channelized between adjacent streamwise jet rows. Thus, the spanwise flow distribution would be nonuniform with velocities between jets larger than those directly approaching the next downstream jet. The degree of nonuniformity would vary with array geometric parameters. Thus, the crossflow velocity seen by a single jet in an array would be smaller than the mean velocity over the cross-section by differing amounts depending on array geometry. Heat transfer coefficients obtained during preliminary tests with a spanwise uniform initial crossflow approaching the array were smaller than those measured at a downstream row of the array without initial crossflow, but total upstream jet flow rate adjusted to provide the same value of G_c/Gi at the downstream row.

Second, the values of Nu being compared for various (x_n/d,y_n/d) combinations are averages over rectangles of widely varying aspect ratios, from x_n/y_n = 0.625 for the (5,8) case where no z/d effect is apparent to 3.75 for the (15,4) case where the effect is significant.

Third, results for potential core length obtained by Stoy and Ben-Haim [6] for a single jet in a confined crossflow indicate that for the present range of z/d, impingement may occur for certain jets before they are developed, and for others (even in the same array) after they are developed.

Effect of Hole Pattern

This effect is illustrated in Fig. 8 where Nusselt numbers for staggered hole patterns normalized by those for their counterpart inline patterns are plotted against the crossflow parameter. The effect is not significant for the largest hole spacing, (x_n/d,y_n/d) = (10,8). However, as x_n/d and y_n/d decrease, and as z/d increases, the staggered pattern results in increasingly reduced heat transfer coefficients relative to the inline values for increasing crossflow.

This behavior is thought to be associated with differences in spanwise distribution of the crossflow in the two cases [2,3]. The tendency of the crossflow to become channelized between adjacent streamwise rows of the inline pattern reduces the direct influence it can exert on each downstream jet. In contrast, the spanwise crossflow distribution presumably remains more nearly uniform for the staggered patterns; hence the crossflow approach velocity directly upstream of each jet is somewhat larger than for the matching inline case.

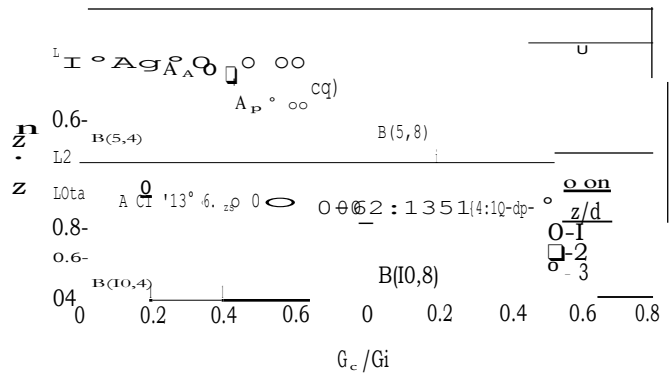

Fig.8 Effect of hole pattern (staggered vs. inline) on streamwise resolved Nusselt numbers as function of crossflow and geometric parameters.

CORRELATION

Correlation attempts were carried out primarily in terms of the variables indicated in Eq. (9). Consideration of the number of these variables (six in all, excluding Prandtl number) coupled with close examination of the data indicated the improbability of achieving a really tight correlation of simple form.

As alluded to earlier, least squares fits of the form $Nu = A\,Bel^{l}$ to data sets for individual sizes at fixed values of the other parameters (G_c/Gj, x_n/d, y_n/d, and z/d) were excellent, though there was an apparently complex but not extremely sensitive variation of m with these parameters.

The plots in Fig. 7, previously examined, indicate that a crossflow functional form representing the dependence on G_e/Gi must, in general, be sensitive to x_n/d, y_n/d, and z/d; and that the sensitivity to z/d varies with x_n/d and y_n/d. Furthermore, plots (not shown) of the same data as in Fig. 7, but rearranged with x_n/d rather than z/d as the parameter within an individual plot show that at $z/d = 1$ the points for $x_n/d = 5$ fall below those for $x_n/d = 10$ which in turn fall below those for $x_n/d = 15$. On the other hand, for $z/d = 2$ and 3 points for $x_n/d = 5$ fall between or above those for $x_n/d = 10$ and 15 depending on the value of y_n/d. Finally, for precise representation such a crossflow functional form would have to be monotonic decreasing for most values of x_n/d, y_n/d, and z/d, but for some cases with $z/d = 1$ would have to allow **a** broad, shallow minimum. Also note that Fig. 8 indicates a different specific correlation is required for the staggered hole pattern, though the same functional form as for the inline pattern may be satisfactory.

A functional form which would properly incorporate in detail all the above features, even if it could be determined, would undoubtedly be extremely cumbersome and complex. After a number of attempts utilizing forms of varying complexity, the following form was finally adopted:

$$Nu = A\,Red\,(1 - B[(z/d)(G_c/G_j)1^{11})1^{3}r^{1}/^{3} \quad (10a)$$

where the coefficients A and B, and the exponents m and n are each permitted to depend on the geometric parameters in the form of simple power functions. That is,

$$A,\ m,\ B,\ \text{and}\ n = C(x_n/d)^{nx}(y_n/d)^{nY}(z/d)^{nz} \quad (10b)$$

The form (10) was applied separately to the inline and staggered hole pattern data for B, C, and D sizes. The analyses were carried out using a multi—variable nonlinear regression routine with a least squares objective function [7]. The objective function was based on the logarithm of the dependent variable (Nu). In this way, the relative deviations rather than the absolute magnitudes were minimized. The resulting best fit values for the coefficients and exponents are summarized in Table 2 for both inline and staggered hole patterns.

The inline correlation, based on a total of 1400 data points, produced a standard error of the deviations of 5.6%. By actual count 95% of the points fall within 11% of the fit line, while 99% fall within 16%. All the points fall within 19%, save one which deviated by 26%. The staggered correlation, based on a total of 680 points, produced a standard error of 6.1%. Ninety—five percent of these points were within 12% of the fit line, 99% were within 16%, and all the points fell within 18%, save one which again deviated by 26%. The bulk of the points having the larger deviations tended to occur for upstream rows for small Re_j at $z/d = 1$.

In an earlier report [3], the degree of consistency of the results obtained for geometrically similar configurations was assessed in detail. Least squares fits in the form Nu = A Red were carried out for the combined data of the several sizes for each set of geometrically similar configurations. In effect, A and m were permitted to be adjustable constants taking different best fit values for each parameter set ($x_n/cLy_n/d, z/d$) and each spanwise row number (i.e., each value of G_c/Gj). Ninety—five percent of the points were within 7% of the respective fit lines, 99% were within 10%, and all were within 14%. These percentages give some indication of the best that might be done if the optimum functional form were to be found. Viewed in this context the proposed correlations appear to be quite acceptable.

The data for the A—size geometries listed in Table 1 were excluded from the data sets relied on for correlation for two reasons. First, the maximum heat transfer coefficient resolution for these data was two rather than one streamwise hole spacings. Second, as previously pointed out [1,3], compressibility effects were present for these cases at the higher Reynolds numbers. This was due to the relatively low laboratory temperature and pressure levels at which the tests were run, combined with the small hole sizes and channel heights for A—size, resulting in pressure drops which were quite large relative to the pressure levels. This leads in some cases to choked flow conditions [1,3].

The pressure and temperature levels in the anticipated turbine application are much higher with correspondingly lower Mach numbers. Therefore, considering the full range of Reynolds numbers, it is expected that the present data for sizes larger than A—size best model the prototype heat transfer characteristics for the gas turbine engine application. Many applications which, in fact, operate at low pressures utilize larger hole sizes and channel heights than for the present A—size. Thus, neither are compressibility effects present to a significant degree in these applications.

It is of interest, nevertheless, to compare the A—size data with the correlation. This was done for Nu resolved to $2x_n$. Despite the Mach numbers for some of these cases approaching or equal to unity, 95% of the points still fall within 16% of the correlation, with only one of 140 points deviating by more than 20% to a value of 27%. (The data used for the A(10,8,1)I case are a revised set recently obtained, which is more consistent with the corresponding B, C, and D size data than the original set documented in [3] and reported in [1]. The reasons for this are explained in [8].)

In developing the correlations, 50 data points for the highest flow rates (ltj from 2.6 to 5.3x10 ⁴) for several B—size configurations were also omitted because choked or nearly choked flow occurred. However, when compared with the correlation 95% of these points are within 15%, the largest deviation being 18%.

Table 2. Constants for use in correlation, Eq. (10)

	Inline Pattern				Staggered Pattern			
	C	nx	ny			nx	ny	nz
A	1.18	-0.944	-0.642	0.169	1.87	-0.771	-0.999	-0.257
m	0.612	0.059	0.032	-0.022	0.571	0.028	0.092	0.039
B	0.437	-0.095	-0.219	0.275	1.03	-0.243	-0.307	0.059
n	0.092	-0.005	0.599	1.04	0.442	0.098	-0.003	0.304

Prior heat transfer measurements involving two—dimensional arrays of circular orifices in which the orifice plate and the heat transfer surface form a channel of uniform height with flow constrained to exit in a single direction parallel to jet hole rows were reported by Friedman and Mueller [9], Huang [10], Kercher and Tabakoff [11], and Chance [12]. These studies reported mean heat transfer coefficients for the entire surface opposite the array [9], or values for spatial resolutions greater than or equal to one streamwise hole spacing [10,11,12]. Only Kercher and Tabakoff, and Chance measured streamwise flow distributions and suggested correlations for streamwise resolved heat transfer coefficients in terms of individual spanwise row jet and crossflow velocities. Kercher and Tabakoff's study included measurements for 16 different combinations of hole spacing and channel height. Only two of these combinations provided streamwise resolutions down to one streamwise hole spacing, and these had just four rows of holes. All were inline arrays with an aspect ratio (x_n/y_n) of unity. Their correlation requires use of three graphical presentations. Chance tested square, equilateral triangular, and rectangular arrays, but did not report specific hole spacings or numbers of holes for his jet plates.

Values of Nu, based on the present correlation are compared with those based on the Kercher and Tabakoff correlation it Fig. 9. The comparison is for square, inline arrays at the extreme values of the geometric parameters which fall within the ranges covered by both investigations. Results based on the correlation of Chance are also shown for cooling of the surface by the jets, which is the same condition under which Kercher and Tabakoff's and the present data were obtained. Chance's correlation for data with heating of the surface falls 10% above that shown in the Figure. The effect of crossflow as calculated from these same correlations is compared in Fig. 10 for the same geometries as Fig. 9.

Permitting both the coefficients and exponents in Eq. (10a) to depend on the geometric parameters provided the flexibility to achieve a reasonably tight overall correlation. This correlation is recommended for detailed analysis and design calculations, particularly when incorporated in computer programs where the larger number of specified constants is not a disadvantage.

An alternate correlation, more convenient for hand computation or examination of trends, is presented below. This correlation is of the same form as (10a), but with exponents m and n not permitted to depend on geometric parameters:

$$Nu/Nu_o = 1 - C(x_n/d)^{nx}(y_n/d)^{ny}(z/d)^{nz}(G_n/G_i)^{n} \quad (11a)$$

where

$$Nu_o = \frac{0.363(x_n/d)^{-0.884}(y_n/d)^{-0.422}(x/d)^{0.054}}{Re^{0.727}Pr^{1/3}} \quad (11b)$$

and the constants in (11a) take the following values:

	C	nx	ny	nz	n
Inline	0.596	−0.103	−0.380	0.803	0.561
Staggered	1.07	−0.198	−0.406	0.788	0.660

This correlation is essentially as good as that of Eq. (10) in terms of standard error and 95% confidence levels, but is not as tight overall.

CONCLUDING REMARKS

Results appropriate for use in analyzing circular jet array impingement systems in which the jet flow is constrained to exit in a single direction along the channel formed by the jet plate and the impingement surface have been developed and presented.

Specifically, row—by—row jet and crossflow velocity distributions may be calculated from Eqs. (7) and (8), which have been verified by experimental results. Knowledge of the jet plate discharge coefficient is required. In the absence of specific values for the particular plates of interest, for jet plates similar to those utilized here a value of 0.79 is recommended.

Heat transfer coefficients resolved to one streamwise hole spacing may be computed from the correlations of either Eq. (10) or (11), for both inline and staggered hole patterns. Knowledge of jet and crossflow velocities at the spanwise row of interest, as well as geometric parameters is required. The heat transfer coefficients on which the correlations are based were measured for a uniform impingement surface temperature.

The parameter ranges on which the results are based are specified in the paper. Caution should be. exercised in extrapolating the results beyond those ranges.

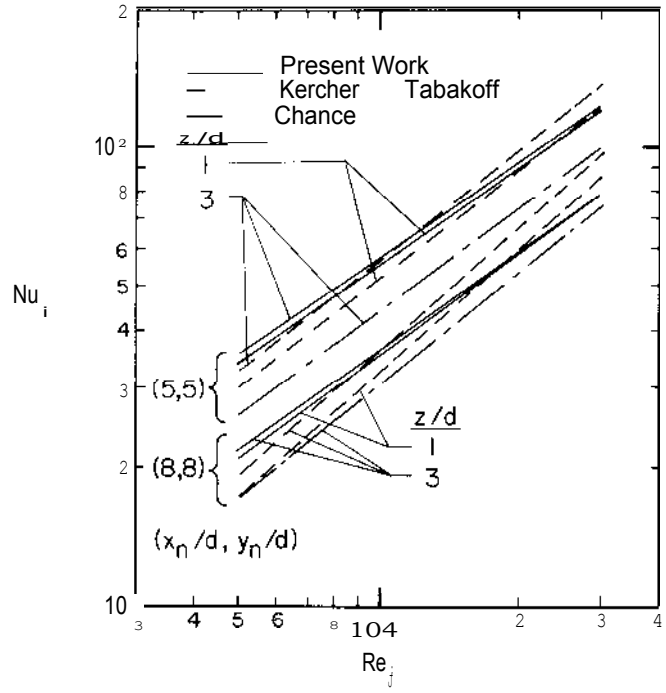

Fig.9 Nusselt number for initial upstream row of array--correlations compared

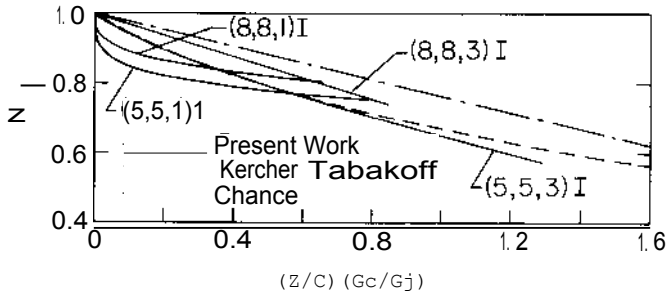

Fig.10 Effect of crossflow on streamwise resolved Nusselt numbers--Correlations compared.

ACKNOWLEDGEMENT

The support of the National Aeronautics and Space Administration, Lewis Research Center, under Grant NSG3075 is hereby gratefully acknowledge.

REFERENCES

1. Metzger, D.E., Florschuetz, L.W., Takeuchi, D.I., Behee, R.D., and Berry, R.A., "Heat Transfer Characteristics for Inline and Staggered Arrays of Circular Jets with Crossflow of Spent Air," ASME Journal of Heat Transfer, Vol. 101, 1979, pp. 526-531.

2. Florschuetz, L.W., Berry R.A., and Metzger, D.E., "Periodic Streamwise Variations of Heat Transfer Coefficients for Inline and Staggered Arrays of Circular Jets with Crossflow of Spent Air," ASME Journal of Heat Transfer, Vol. 102, 1980, pp. 132-137.

3. Florschuetz, L.W., Metzger, D.E., Takeuchi, D.I., and Berry, R.A., Multiple Jet Impingement Heat Transfer Characteristics -- Experimental Investigation of Inline and Staggered Arrays with Cross—flow, NASA—CR-3217, Arizona State University, Tempe, January 1980.

4. Martin, H., "Heat and Mass Transfer Between Impinging Gas Jets and Solid Surfaces," Advances in Heat Transfer, Vol. 13, Academic Press, New York, 1977, pp 1-60.

5. Metzger, D.E., and Korstad, R.J., "Effects of Cross Flow in Impingement Heat Transfer," ASME Journal of Engineering for Power, Vol. 94, 1972, pp. 35-41.

6. Stoy, R.L., and Ben—Haim, Y., "Turbulent Jets in a Confined Crossflow," ASME Journal of Fluids Engineering, Vol. 95, 1973, pp. 551-556.

7. Kuester, J.L., and Mize, J.H., Optimization Techniques with Fortran, McGraw—Hill, New York, 1973, pp. 240-250.

8. Florschuetz, L.W., Metzger, D.E., and Truman, C.R., "Jet Array Impingement with Crossflow -- Correlation of Streamwise Resolved Flow and Heat Transfer Distributions," NASA Contractor Report, Department of Mechanical Engineering, Arizona State University, Tempe, in press.

9. Friedman, S.J., and Mueller, A.C., "Heat Transfer to Flat Surfaces," Proceedings, General Discussion on Heat Transfer, The Institute of Mechanical Engineers, London, England, 1951, pp. 138-142.

10. Huang, G.C., "Investigations of Heat Transfer Coefficients for Air Flow Through Round Jets Impinging Normal to a Heat Transfer Surface," ASME Journal of Heat Transfer, Vol. 85, 1963, pp. 237-243.

11. Kercher, D.M., and Tabakoff, W., "Heat Transfer by a Square Array of Round Air Jets Impinging Perpendicular to a Flat Surface Including the Effect of Spent Air," ASME Journal of Engineering for Power, Vol. 92, 1970, pp. 73-82.

12. Chance, J.L., "Experimental Investigation of Air Impingement Heat Transfer Under an Array of Round Jets," Tappi, Vol. 57, No. 6, 1974, pp. 108-112.